



# Taming Lagrangian chaos with multi-objective reinforcement learning

Chiara Calascibetta<sup>1,a</sup> , Luca Biferale<sup>1</sup>, Francesco Borra<sup>2</sup>, Antonio Celani<sup>3</sup>, and Massimo Cencini<sup>4,5</sup>

<sup>1</sup> Department of Physics & INFN, University of Rome ‘Tor Vergata’, Via della Ricerca Scientifica 1, 00133 Rome, Italy

<sup>2</sup> Laboratory of Physics of the École Normale Supérieure, 24 RueLhomond, 75005 Paris, France

<sup>3</sup> Quantitative Life Sciences, The Abdus Salam International Centre for Theoretical Physics, ICTP, 34151 Trieste, Italy

<sup>4</sup> Istituto dei Sistemi Complessi, CNR, Via dei Taurini 19, 00185 Rome, Italy

<sup>5</sup> INFN ‘Tor Vergata’, Rome, Italy

Received 19 December 2022 / Accepted 15 February 2023 / Published online 3 March 2023

© The Author(s), under exclusive licence to EDP Sciences, SIF and Springer-Verlag GmbH Germany, part of Springer Nature 2023

**Abstract** We consider the problem of two active particles in 2D complex flows with the multi-objective goals of minimizing both the dispersion rate and the control activation cost of the pair. We approach the problem by means of multi-objective reinforcement learning (MORL), combining scalarization techniques together with a Q-learning algorithm, for Lagrangian drifters that have variable swimming velocity. We show that MORL is able to find a set of trade-off solutions forming an optimal Pareto frontier. As a benchmark, we show that a set of heuristic strategies are dominated by the MORL solutions. We consider the situation in which the agents cannot update their control variables continuously, but only after a discrete (decision) time,  $\tau$ . We show that there is a range of decision times, in between the Lyapunov time and the continuous updating limit, where reinforcement learning finds strategies that significantly improve over heuristics. In particular, we discuss how large decision times require enhanced knowledge of the flow, whereas for smaller  $\tau$  all a priori heuristic strategies become Pareto optimal.

## 1 Introduction

In many engineering and geophysical applications, robotic instruments are often used for multi-agent sensing, e.g., where a fleet of instrumented drifters is used to collect information in the ocean, multi-robots are used for searching sources leaking hazardous substances, or to probe complex environments [1–5]. A typical application is how to keep the fleet under control, e.g., for patrolling the same region, keeping a given geometric formation and/or following a predetermined point-to-point path. In typical flows, the relative distance between two passive drifters would always grow, either exponentially, due to Lagrangian chaos when they are close, or in a diffusive way at large scales, when nonlinear effects become dominant [6, 7]. Animal behavior is often an inspiration and a leading direction of research trying to develop bio-mimetic strategies [8–10]. However, it is unclear whether using heuristic hard-wired rules would be enough to control the swarm in the presence of a strongly mixing flow [11]. Moreover, in

many realistic applications, agents need to take into account of strong engineering or biological limitations, needing to actively learn how to take advantage of the flow to accomplish the goal. As a result, we search to develop active complex policies to control complex environments. In chaotic or turbulent flows, the problem is given by the strong sensitivity of the system to any perturbation, making the very meaning of optimal control a fragile notion. In this direction, a few attempts to control single Lagrangian instrumented particles via reinforcement learning (RL) algorithms have been proposed to solve the Zermelo’s optimal navigation problem of reaching a fixed target [12–14]. Moreover, RL has been successfully employed to optimize the soaring of a glider in thermal currents [15, 16], to harness wind for airborne energy [17] and to optimize collective swimming by harnessing vortices [18]. Optimal navigation is also important in biological systems, e.g., for developing microswimmers with adaptive locomotory gaits [19] and learning how to actively steer in response to hydrodynamic signals [20, 21]. Recently, adversarial games between two competing agents have also been proposed to study chase-and-escape strategies at low Reynolds number [22], while strategies from both Optimal Control and RL point of view have been explored for a finite-size swimming predator chasing a nonmotile prey [23]. Instead, with an analytical analysis, the role

T.I.: Quantitative AI in Complex Fluids and Complex Flows: Challenges and Benchmarks. Guest editors: Luca Biferale, Michele Buzicotti, Massimo Cencini.

<sup>a</sup> e-mail: [calascibetta@roma2.infn.it](mailto:calascibetta@roma2.infn.it) (corresponding author)

of noise for an active Brownian particle approaching a moving target has been explored in [24].

In this paper, we consider two agents (a particle pair) transported by a flow and having some limited knowledge on the underlying flow, which should act collectively so as to contrast the growth of their separation and, at the same time, to minimize as much as possible the cost for control. We assumed to solve the problem when the two particles stay at distances where the flow is differentiable so that, without control, their separation would grow exponentially due to Lagrangian chaos. To improve realism, we model the problem imposing limitations in detection (partial observability) and in the possible actions to undertake (partial maneuverability). Namely, we allow each agent to sample only few local properties of the underlying flow and to receive information about the other one only at given *decision times*, spaced by an interval  $\tau$ , in order to update their actions. For what concerns the actions, following [14] we suppose that the two objects can swim either along the direction of their separation or in the perpendicular one, with a variable speed. Finally, to be able to fulfill the objective to minimize the control activation cost, we also include the action of *no-swimming* to allow the couple of particles to learn when to be passively transported by the current, if useful [13]. As a result, we have a multi-agent (a Lagrangian pair) and a multi-task (minimize both chaotic dispersion and activation cost) problem [25]. We approach this typical long-term optimization problem with conflicting objectives by using Multi-Objective reinforcement learning (MORL) algorithms [26–28]. Indeed, in the classical single-task RL the reward is a scalar, whereas in MORL the reward is a vector, with an element for each objective. We approach MORL via scalarization, i.e., by defining a new scalar total reward by a weighted sum along all the element of the original reward vector [29,30]. For this reason, there exists a set of trade-off solutions forming the so called Pareto frontier [31,32], where each solution on the frontier is Pareto Efficient, i.e., no single objective can be made better off without making at least another one worse off.

Using this approach, we show how to find a set of Pareto optimal policies to efficiently minimize both chaotic dispersion and swimming cost. To benchmark these strategies, we will compare them to a set of heuristic baselines. In particular, we show how the learned strategies are able to exploit nontrivial information of the underlying flow.

The paper is organized as follows. In Sect. 2, we describe the general setup of the problem: the model of the Lagrangian pair, how they can act and sense the environment, and the details of the underlying fluid flow. In Sect. 3, we introduce the concepts of MORL giving details on our choice for the reward function and the learning protocol. Furthermore, we present the concepts of Pareto dominance and Pareto frontier. In Sect. 4, we discuss the main results including a heuristic analysis focused on explaining the role of the *decision time*. Finally, we give our conclusion in Sect. 5.

## 2 The model

### 2.1 Active control of Lagrangian pairs in a flow

In typical flows, Lagrangian chaos [6,7] causes an exponential growth of the separation,  $\delta X(t) = \|\mathbf{X}_2(t) - \mathbf{X}_1(t)\|$ , between pairs of (uncontrolled) tracer particles that are initially very close, i.e.,  $\langle \ln \delta X(t) \rangle \simeq \ln \delta X(0) + \lambda t$ , ( $\lambda$  being the Lagrangian Lyapunov exponent). Our goal here is to develop strategies for instrumented particles to control and, possibly, minimize such chaotic dispersion and at the same time to save activation cost. In particular, we consider particles in the one-way coupling approximation and an autonomous propelling mechanism with a speed  $V(t)$  in the direction  $\hat{\mathbf{p}}(t)$  superimposed to the transport by the flow. Thus we assume the particles to obey the following equations of motion:

$$\begin{cases} \dot{\mathbf{X}}_\alpha = \mathbf{u}(\mathbf{X}_\alpha(t), t) + \mathbf{U}_\alpha^{ctrl}(t), \\ \mathbf{U}_\alpha^{ctrl}(t) = V_\alpha(t) \hat{\mathbf{p}}_\alpha(t), \end{cases} \quad (1)$$

where  $\alpha = 1, 2$  is the agent's index,  $\mathbf{u}(\mathbf{X}_\alpha(t), t)$  is the velocity of the underlying 2D advecting flow and  $\mathbf{U}_\alpha^{ctrl}(t)$  is the control contribution to the particle velocity. In Eq. (1), we neglect the rotation kinematics of  $\hat{\mathbf{p}}_\alpha$  assuming the agents equipped with an active and instantaneous reorientation mechanism. Thus, we consider the reorientation time negligible and the current swimming direction always aligned with the chosen one.

We assume the agents to interact between each other only every  $\tau$  time units. At each decision time, the agents can measure some flow properties (a proxy for the environmental *state*) and sense their mutual separation. Then, on the basis of the information received, they can decide their *action*, i.e., choose the swimming intensity and direction. In this way, the control  $\mathbf{U}_\alpha^{ctrl}(t)$  becomes a piece-wise constant in time function, i.e.,  $\hat{\mathbf{p}}_\alpha(t) = \hat{\mathbf{p}}_\alpha(t_j)$  and  $V_\alpha(t) = V_\alpha(t_j)$  for  $t_j \leq t < t_j + \tau$ , with  $t_j = j\tau$  being the  $j^{th}$  decision time. Clearly, an important role in achieving successfully strategies for staying close is played by the dimensionless combination of the two parameters  $\tau\lambda$ . When  $\tau\lambda > 1$ , the control is too sporadic and the velocity field can separate considerably the agents. On the other hand, for  $\tau\lambda \rightarrow 0$ , the control problem becomes easier.

Concerning the swimming directions,  $\hat{\mathbf{p}}_\alpha(t)$ , we assume that the agents have a limited set of choices. Namely, similarly to [14], the agents can either swim along their longitudinal (joining) direction ( $\hat{\mathbf{n}}_\parallel$ ) or in the transversal one ( $\hat{\mathbf{n}}_\perp$ ). Where  $\hat{\mathbf{n}}_\parallel = (\mathbf{X}_2 - \mathbf{X}_1)/\delta X$  and  $\hat{\mathbf{n}}_\perp \cdot \hat{\mathbf{n}}_\parallel = 0$  (see Fig. 1). To make the problem interpretable from a dynamical system theory point of view, we set the swimming intensity,  $V_\alpha(t)$  to be proportional to the agents' distance (measured at the decision time), i.e.,

$$V_\alpha(t) = F_\alpha(t) \delta X(t), \quad (2)$$

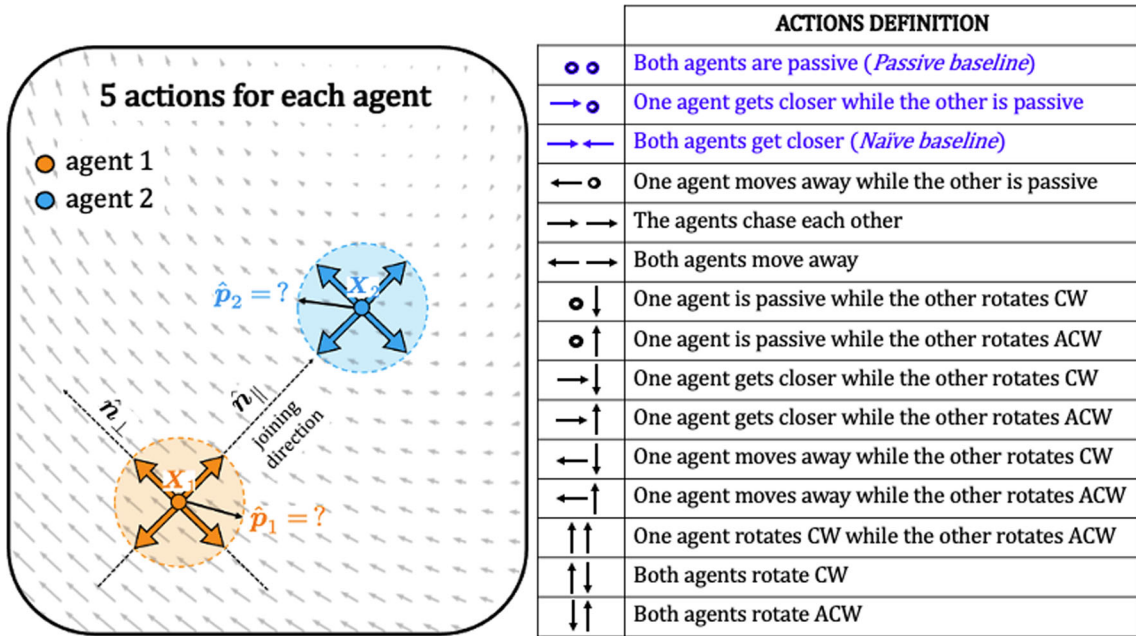


**Fig. 1** (Left) Artistic view of the problem. Two agents in a linear regime transported by a flow that tends to rotate their separation vector clockwise (CW). We show the 5 possible actions available to each agent, namely: remain passive or swim in the longitudinal direction  $\pm \hat{n}_{\parallel}$  or in the

transversal one  $\pm \hat{n}_{\perp}$ . (Right) Scheme of the set of 15 actions for the couple of agents, obtained after removing symmetrical action pairs. Besides the longitudinal actions, choosing the transversal directions allows the agents to rotate with respect to each other clockwise (CW) or ACW

and we let each agent to choose either to turn on the control by actively swimming,  $F_{\alpha}(t) = f > 0$ , or to turn it off,  $F_{\alpha}(t) = 0$ , to save activation cost. With this choice, the two objectives are directly connected with the minimization of the Lyapunov exponent of the controlled system. This allowed us to derive the heuristic analysis described in Sect. 4.2 and to predict the Pareto frontier in the limit  $\tau \rightarrow 0$ , see Eq. (15). Furthermore, from a theoretical point of view it is interesting and challenging per se to understand how to optimize the dynamics under many possible constraints,  $V_{\alpha}(t) \propto \delta X(t)$  in this case. In the future, it could be interesting to study the system with different setups, varying both the actions (e.g., imposing a maximum swimming velocity), the state-space and the definition of the cost function. At the same time, had we used a constant swimming speed, would have introduced a typical threshold distance above/below which the agents will always be able to control/not-control, at least, for small values of  $\tau$ . Furthermore, to study the problem in a more challenging way, we assume that swimming cannot completely overcome the dynamics, i.e.,  $2f \lesssim \lambda$  (see below).

Summarizing, at each decision time  $t_j$ , agent  $\alpha$  can pick any of 5 actions,  $a \in \{F_{\alpha}(t_j) = 0; F_{\alpha}(t_j) = f$  with  $\hat{p}_{\alpha} = \pm \hat{n}_{\parallel}, \pm \hat{n}_{\perp}\}$  namely, the agents can choose either to be passive or to swim along their longitudinal or perpendicular directions. We will call *naïve policy* the strategy where the agents always choose to navigate toward each other, i.e.,  $\hat{p}_1 = \hat{n}_{\parallel}$  and  $\hat{p}_2 = -\hat{n}_{\parallel}$ . Likewise, we will call *passive policy* the strategy when

$F_1 = F_2 = 0$ . In principle, a set of  $5^2 = 25$  actions is available for the couple of agents. However, the space of actions can be reduced by removing symmetries (e.g., the configuration in which  $\hat{p}_1 = \hat{n}_{\parallel}$  and the second is passive is equivalent to the configuration in which the first agent is passive and  $\hat{p}_2 = -\hat{n}_{\parallel}$ ). In this way, the set of actions for the couple reduces to the set  $\mathcal{A}$  of 15 actions shown in Fig. 1.

### 2.2 Sensing the environment

Besides their relative position and distance, at each decision time, the agents receive some cues on the fluid environmental state. Concerning the observability of the environment, assuming that they are close enough for the field to be smooth, we imagine the two agents can have only a rough estimates of the relative longitudinal and transverse gradients, defined as

$$\sigma_{\parallel} = \frac{(\mathbf{u}(\mathbf{X}_2, t) - \mathbf{u}(\mathbf{X}_1, t))}{\delta X} \cdot \hat{n}_{\parallel} \tag{3}$$

$$\sigma_{\perp} = \frac{(\mathbf{u}(\mathbf{X}_2, t) - \mathbf{u}(\mathbf{X}_1, t))}{\delta X} \cdot \hat{n}_{\perp}, \tag{4}$$

which can be obtained by exchanging information about their local velocities. To search for interpretable solutions, we restrict the state-space supposing that the agents are able to measure the gradients (3)(4) with a limited sensitivity. In particular, we restrict the set of values of  $\sigma_{\perp}, \sigma_{\parallel}$  to 4 states for each one of them, for a total of 16 discretized states, labeling whether the

	contracting <span style="color: red;">→</span> expanding			
CW	$\sigma_{\parallel} < -c$	$-c \leq \sigma_{\parallel} < 0$	$0 \leq \sigma_{\parallel} < c$	$\sigma_{\parallel} \geq c$
	$\sigma_{\perp} < -c$	$\sigma_{\perp} < -c$	$\sigma_{\perp} < -c$	$\sigma_{\perp} < -c$
	$\sigma_{\parallel} < -c$	$-c \leq \sigma_{\parallel} < 0$	$0 \leq \sigma_{\parallel} < c$	$\sigma_{\parallel} \geq c$
	$-c \leq \sigma_{\perp} < 0$	$-c \leq \sigma_{\perp} < 0$	$-c \leq \sigma_{\perp} < 0$	$-c \leq \sigma_{\perp} < 0$
ACW	$\sigma_{\parallel} < -c$	$-c \leq \sigma_{\parallel} < 0$	$0 \leq \sigma_{\parallel} < c$	$\sigma_{\parallel} \geq c$
	$0 \leq \sigma_{\perp} < c$	$0 \leq \sigma_{\perp} < c$	$0 \leq \sigma_{\perp} < c$	$0 \leq \sigma_{\perp} < c$
	$\sigma_{\parallel} < -c$	$-c \leq \sigma_{\parallel} < 0$	$0 \leq \sigma_{\parallel} < c$	$\sigma_{\parallel} \geq c$
	$\sigma_{\perp} \geq c$	$\sigma_{\perp} \geq c$	$\sigma_{\perp} \geq c$	$\sigma_{\perp} \geq c$

**Fig. 2** Definition of the 16 states, obtained from the discretization of longitudinal (3) and transversal (4) gradients. The former informs about the local rate of expansion/contraction due to the flow, the latter tells the rate of clockwise (CW) or anticlockwise (ACW) rotation imposed by the flow on the joining direction. In figure are shown the states discretization with thresholds 0 and  $\pm c$

underlying flow brings them closer or farther away (longitudinal gradients) and in which direction it rotates them (transverse gradients) see Fig. 2 for a summary of all states. The value of the discretization constant  $c$  is chosen so that all the 16 states are sufficiently visited ( $c = 2.8$  in our case). Setting  $c$  too small or too high would practically reduce the state-space from 16 to 4 resulting in sub-optimal policies with respect to the ones obtained from the 16 almost-uniformly visited states.

### 2.3 The space of control policies

Given 15 actions and 16 states, we have a possible set of  $15^{16}$  deterministic policies  $[\pi : s \rightarrow a]$ , making the brute force optimization search impossible: one has to resort to reinforcement learning techniques (as discussed in Sect. 3). However, there is an intuitive way to trace back to a reduced policies space that can be analyzed systematically as a set of hard-wired baseline policies. By restricting perceptions to the longitudinal components (3), we can assume that only the actions along the joining direction are important. Considering only the first three actions highlighted in blue in the right panel of Fig. 1, we get to a reduced set  $3^4 = 81$  policies, which will be used in the following as our reference heuristics to benchmark those found by MORL implementation.

### 2.4 Model flow

As for the fluid environment, we used a 2D homogeneous, (nearly) isotropic, incompressible and time-dependent flow as in Ref. [33]. In particular, the velocity field is defined in terms of a stream function,  $\mathbf{u}(\mathbf{x}, t) = \nabla_{\perp} \psi(\mathbf{x}, t) = (\partial_y \psi, -\partial_x \psi)$ , which is expressed as a superposition of few Fourier modes,

$$\psi(\mathbf{x}, t) = \sum_{\mathbf{k} \in \mathcal{K}} (A(\mathbf{k}, t)e^{i\mathbf{k} \cdot \mathbf{x}} + cc.), \quad (5)$$

$\mathcal{K} = \{(\frac{2\pi}{L}, 0), (\pm \frac{2\pi}{L}, \frac{2\pi}{L}), (0, \frac{2\pi}{L})\}$ , where  $L$  is the scale periodicity of the flow. In (5)  $A(\mathbf{k}, t) = A_r(\mathbf{k}, t) + iA_i(\mathbf{k}, t)$  are random and time-dependent amplitudes obtained from an Ornstein–Uhlenbeck process [34]

$$\dot{A}_{\beta}(\mathbf{k}, t) = -\frac{1}{\tau_f} A_{\beta}(\mathbf{k}, t) + \left(\frac{2\sigma^2(\mathbf{k})}{\tau_f}\right)^{1/2} \eta_{\beta}(\mathbf{k}, t), \quad (6)$$

with  $\beta = r, i$ . Here  $\tau_f$  sets the flow correlation time,  $\eta_{\beta}(\mathbf{k}, t)$  are zero-mean Gaussian variables with correlation  $\langle \eta_{\alpha}(\mathbf{k}, t)\eta_{\beta}(\mathbf{k}', t') \rangle = \delta_{\alpha, \beta} \delta_{\mathbf{k}, \mathbf{k}'} \delta(t - t')$ , and  $\sigma^2(\mathbf{k}) = \frac{u_{rms}^2}{2\|\mathbf{k}\|^2}$ . We fixed  $\tau_f = 1, L = 1, u_{rms} = 1$ . With this choice, the maximum Lyapunov exponent characterizing the mean exponential rate of divergence between two (uncontrolled) tracers particles (passive strategy) is  $\lambda \simeq 1.4$ .

### 3 Reinforcement learning and multi-objective optimization

Starting from our set of states and actions, our aim is to solve an optimization problem with two objectives: minimizing both the rate of separation growth and the activation cost. We are thus in the field of competing Multi-Objective Optimization (MOO) [25, 26]. The optimality of such solutions can be defined in terms of Pareto dominance [28, 32], namely a solution dominates another if it is superior on at least one objective and at least equal on all others. For instance, in Fig. 3a) the solutions  $M$  and  $K$  dominate  $J$ , whereas  $M$  and  $K$  are incomparable, because each is superior in at least one objective. All the dominating solutions form the Pareto frontier [28, 32], depicted with black circles in Fig. 3b).

Reinforcement learning (RL) algorithms [35] aim at maximizing a single scalar reward usually representing a single long-term objective. MOO can also be obtained within standard RL algorithms such as, e.g., Q-learning [35] by scalarization, formulating a “new” total single-objective optimization problem obtained as a weighted sum of each sub-objective functions [29, 30]. By solving the scalar optimization problem at varying the weights in the sum, one can find the Pareto optimal solutions to the MOO. Following this idea, we define a different reward function for each of the two competing sub-problems.

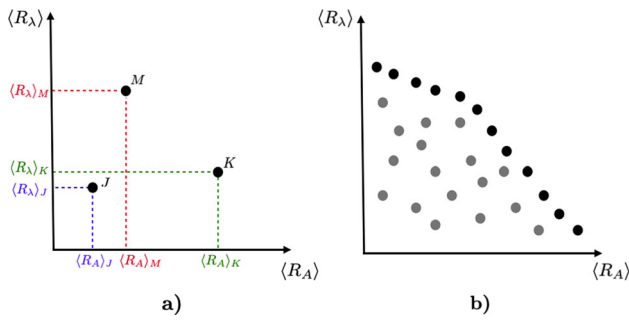


**Fig. 3** Concepts of Pareto dominance (a) and Pareto frontier (b).  $\langle R_\lambda \rangle$  and  $\langle R_A \rangle$  represent the two single objectives of minimizing particle separation and activation cost

The first allows the agents to judge their performance in controlling the separation rate:

$$r_\lambda(t_j) = -\frac{1}{T_{\max}} \ln \left( \frac{\delta X(t_j)}{\delta X(t_j - \tau)} \right), \tag{7}$$

which penalizes actions that, between two consecutive decisions, cause an increase of the distance, and where  $T_{\max}$  is a fixed time horizon that we considered as terminal state for the learning episodes and chosen such that the relative distance between the two particles is always in the linear regime ( $T_{\max} = 5.5$  in our case). Notice that summing the reward (7) over a whole episode

$$R_\lambda = \sum_{j=1}^{T_{\max}/\tau} r_\lambda(t_j) \tag{8}$$

when averaging over many episodes we have

$$\langle R_\lambda \rangle = -\frac{1}{T_{\max}} \left\langle \frac{\delta X(T_{\max})}{\delta X(0)} \right\rangle \simeq -\lambda_c. \tag{9}$$

Thus, the optimization problem restricted to this reward would be solved by the policy which minimizes the Lyapunov exponent of the controlled system,  $\lambda_c$ .

The second reward function informs the agent about the activation cost:

$$r_A(t_j) = -\frac{1}{T_{\max}} \lambda \tau N_a(t_j) \tag{10}$$

where  $N_a(t_j) (= 0, 1, 2)$  counts the number of agents which have selected any of the actions ‘swim’; we have introduced a normalization term  $\lambda \tau$  to have two rewards of the same order of magnitude (on average we can estimate  $r_\lambda = (\tau \lambda) / T_{\max}$ ).

For the multi-objective optimization, we need to combine (7) and (10) through a scalarization parameter,  $\beta$ :

$$r_{\text{tot}}(t_j) = r_\lambda(t_j) + \beta r_A(t_j) \tag{11}$$

and consider many single-objective problems for  $r_{\text{tot}}$  at varying  $\beta$ . Therefore, at each decision time, the

Lagrangian pair receives a shared reward,  $r_{\text{tot}}$ . For each  $\beta$ , the goal is to find the policy maximizing the cumulative total reward,

$$R_{\text{tot}} = \sum_{j=1}^{T_{\max}/\tau} [r_\lambda(t_j) + \beta r_A(t_j)] = R_\lambda + \beta R_A. \tag{12}$$

From the above expression, there are two clear limits:  $\beta \rightarrow 0$  and  $\beta \rightarrow \infty$ . In the former limit, we minimize particle distance without caring on activation cost, a goal that is not obvious *per se* and will depend on the decision time,  $\tau$ . The latter case is simpler, because as the cost of swimming increases the best policy is the passive one. How does the transition between these two limiting regimes takes place is the question that we are going to answer in Sect. 4 by studying the Pareto frontier of our multi-task problem. See Appendix 1 for details of the Q-learning algorithm that we have implemented.

Due to learning stochasticity and the fact that the performances of different policies can be very close, to find the best solutions we performed 100 independent learning sections (i.e., using different initialization seeds) for each scalarization parameter  $\beta$ . Each learning section lasts 50,000 episodes. The 100 learned policies for each  $\beta$  have been validated on 100,000 different realizations of the flow. Then we assumed as *best learned policies* the ones that maximize the average over the validation set of (12).

### 4 Results

Here, we present the results. In the first section, we present a detailed analysis of the policy related to a fixed decision time value,  $\tau = 0.3$ , which gives that the uncontrolled Lyapunov exponent is  $\lambda \approx 1.4$  corresponding to a case  $\tau \lambda < 1$  (and  $\tau < \tau_f = 1$ ) that allows us to control the dynamics but the interval between decision times,  $\tau$ , is sufficiently high to make the problem nontrivial. In the second section, we analyze specifically the role of  $\tau$  presenting a heuristic analytical prediction in the  $\tau \rightarrow 0$  limit and a numerical study based on the heuristic policies as a function of  $\tau$ . In particular, we show that the concavity of the Pareto frontier is strongly dependent on  $\tau$ .

To make the control nontrivial, we fix the swimming rate to  $f = 0.7$  so that the controlled Lyapunov exponent is close to 0 for  $\beta = 0$  and  $\tau \rightarrow 0$  and never negative for other  $\beta, \tau$  values. For smaller values of  $f$ , we have obtained qualitatively similar results (not shown), even though controlling the separation becomes much more complicated also for  $\beta = 0$ . Higher values of  $f$ , instead, make the system trivially controllable.

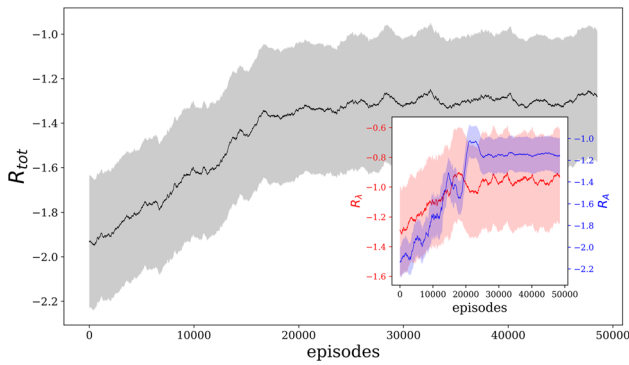


**Fig. 4** Example of learning process. The total reward  $R_{tot}$  versus the episodes: the solid line and gray shaded area show the running average and fluctuations over 1500 episodes, respectively. The inset shows the evolution of the two contributions to the reward  $R_\lambda$  (red) and  $R_A$  (blue). Data refer to one learning trial for  $\beta = 0.3$  and  $\tau = 0.3$

### 4.1 Detailed analysis of learned policies

As discussed in Sect. 3, we approach the multi-objective optimization through reinforcement learning via scalarization, that is we perform many learning processes, with the protocol described at the end of Sect. 3, by varying the scalarization parameter  $\beta$  that weighs the two rewards (see (12)). In Fig. 4, we show a typical learning process for a single  $\beta$  value. At the beginning of the learning phase, the Q-learning algorithm explores different random policies. After many episodes, the learning parameters,  $\epsilon$  and  $\alpha$ , decrease (see (19)–

(20)) and the Q-matrix stabilizes. The inset of Fig. 4 displays the evolution of two components of the reward. As discussed, for the same  $\beta$  the learning process is then repeated over 100 trials, each learned policy is evaluated on a validation set to identify the best learned policy for that value of  $\beta$ .

In Fig. 5, we show the mean (over the validation set) of the total cumulative reward obtained to minimize the separation,  $\langle R_\lambda \rangle$  (9) versus the mean of the total cumulative reward obtained to save control activation cost,  $\langle R_A \rangle = \left\langle \sum_{j=1}^{T_{max}/\tau} r_A(t_j) \right\rangle$ , for different  $\beta$  values. Then we can identify as optimal the solutions that dominate all the others in the sense of Pareto dominance. In particular, the best learned policies for each  $\beta$  are surely on the Pareto frontier (filled circles in Fig. 5). As one can see, the learned policies reach rewards that outperform the 81 heuristic policies, indicating that the RL protocol has converged to optimal solutions. The inset in Fig. 5 provides a quantitative idea of the improvement with respect to the *naïve* and passive baseline, respectively, by showing the improvement of the best learned policies as a function of  $\beta$ . One can see that the best learned policies are generically better than the baselines.

In particular, for  $\beta = 0$ , since there is no cost for swimming, one might expect the *naïve* baseline to be a good strategy for minimizing the agents separation. Instead, we discovered that also in this limit there is a nontrivial optimal strategy for Lagrangian agents that outperform the *naïve* one with an improvement of 12% in the maximization of the total reward. The discovered strategy is such that, when the velocity field is con-

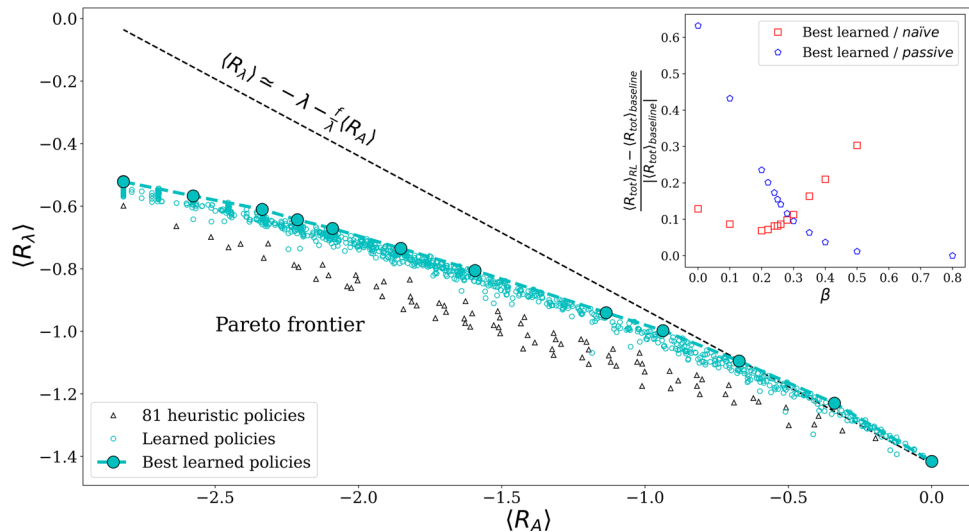


**Fig. 5**  $\langle R_\lambda \rangle$  versus  $\langle R_A \rangle$  obtained by setting the decision time  $\tau = 0.3$ . The dashed black line indicates the highest performances that can be achieved for  $\tau \rightarrow 0$  (see (15)). We show with black triangles the performances of 81 heuristic policies and with light blue circles all the policies learned by the Q-learning algorithm to solve the multi-objective problem, in particular the filled large circles show the best

learned policies for each  $\beta$ , and the dashed blue line the highest Pareto frontier. One can see that learned policies dominate the heuristic ones. Inset: Relative improvement of  $\langle R_{tot} \rangle$  as a function of  $\beta$  of the best policies learned from RL with respect to the *naïve* (red squares) and passive (blue pentagon), respectively

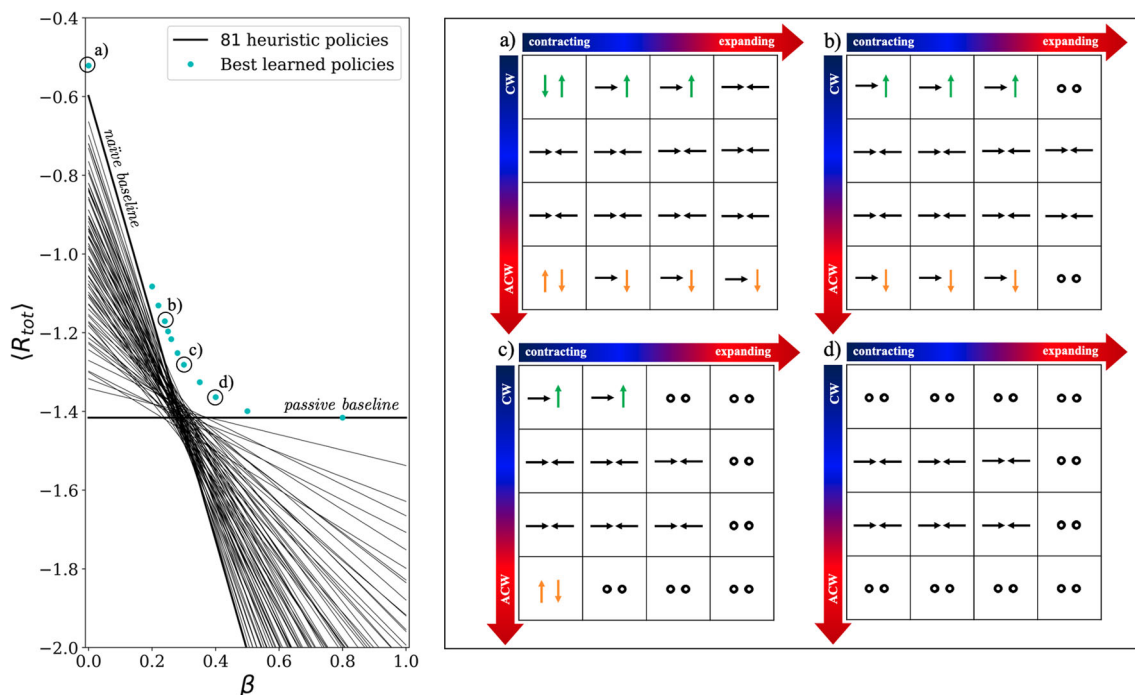


**Fig. 6** (Left)  $\langle R_{tot} \rangle$  versus  $\beta$  for different policies obtained with a decision time  $\tau = 0.3$ . With the 81 straight lines are shown the heuristic performances, including the two extreme cases of the naïve baseline and the passive policy. It can be seen that as  $\beta$  increases the naïve policy immediately get worse, while the passive policy is  $\beta$ -independent. In light blue are shown the best policies learned from Q-learning for

each  $\beta$  that improve all the heuristic performances. (Right) Pictorial representation of 4 policies learned from RL corresponding to the circled symbols on the left. In green and orange are highlighted the ACW and CW rotation actions chosen as a counter-move with respect to the underlying flow rotation

tracting and rotates strongly the position of one agent with respect to the other, it turns out to be more convenient to counter-rotate with respect to the rotation induced by underlying velocity field rather than to simply navigate toward each other. We can explain that as a realignment along the contracting direction. Indeed, due to the finite decision time, it is less effective to swim toward each other in the direction identified at the decision time, which is quickly changed by the flow. On the other hand, for high values of  $\beta$ , when swimming has a high cost, RL easily learns that the best policy is the passive one, where the two agents always switch off the engine. Other  $\beta$  values lead to the transition region between these two extreme cases, where new navigation strategies are learned. In particular, as seen from the inset of Fig. 5, the region around  $\beta = 0.3$  seems to be the more interesting, and it is thus worth analyzing the learned policies in this region.

In Fig. 6(Left), we show the performance of the best learned policies for each  $\beta$  in comparison with the 81 heuristic ones. Notice that for the latter it is enough to measure  $\langle R_\lambda \rangle$  and  $\langle R_A \rangle$  to know the value of  $\langle R_{tot} \rangle$  as a function of  $\beta$ , obtaining 81 benchmark straight lines, as shown in Fig. 6(Left). It can be seen that RL always improves the maximization of the total cumulative reward,  $\langle R_{tot} \rangle$ . In Fig. 6(Right)a–d, we show a tabular representation of some policies learned as optimal, i.e., that lie on the Pareto frontier and appertain to the

region around  $\beta = 0.3$  (see circled dots in Fig. 6(Left)). It emerges that counter-rotating with respect to the underlying flow rotation is important and that, as  $\beta$  increases, is more convenient to navigate when the flow is contracting rather than when it is expanding the agents' separation, e.g., the policy in Fig. 6c) shows that the Lagrangian pair choose to be passive along all the expanding states.

We end this section commenting on possible symmetries of swimming strategies. In fact, the counter-rotating action with respect to the underlying flow rotation, which emerges to be important, can occur both when the counter-rotation is clockwise and when it is anticlockwise. Even though symmetric strategies can exist simultaneously, we found that RL is able to converge to optimal solutions. In particular, the policies shown in the panels b) and d) of Fig. 6 are exactly symmetric, while the policies in a) and c) are only approximately symmetric. In fact, in a) we have the agents navigating toward each other (naïve strategy) in the state in the first-row fourth-column (i.e., (1,4) state), while in the symmetric state (4,4) one agent is counter-rotating with respect to the underlying flow rotation. Similarly, in c) the actions in the (1,2) state and in its symmetric (4,2) are different. Analyzing the performances of the symmetric counterparts of these policies (i.e., for example, considering for a) one agent counter-rotating with respect to the flow in the (1,4) state and both

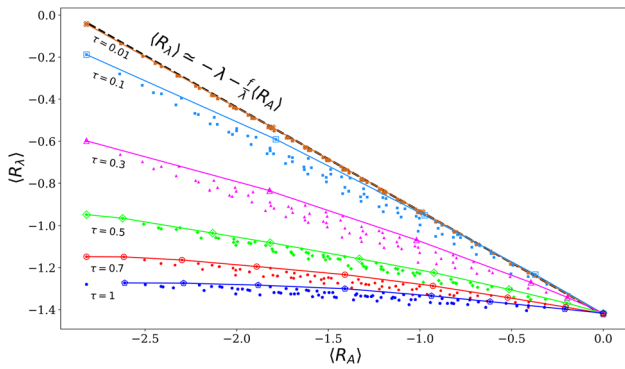


**Fig. 7** Pareto frontier for a *reduced policies space*, which is a lower bound to the true Pareto frontier:  $\langle R_\lambda \rangle$  versus  $\langle R_A \rangle$  obtained varying the decision time,  $\tau$  for the 81 heuristic policies. The dashed black line indicates a linear dependence between  $\langle R_\lambda \rangle$  and  $\langle R_A \rangle$  reached for small  $\tau$ . We show with empty symbols the Pareto frontier that would result for each decision time by restricting the problem to study only the 81 heuristic policies. It can be seen that as  $\tau$  increases, the frontier becomes concave

the agents swimming toward each other (*naïve* policy) in the (4,4) state) we found that symmetric strategies are actually equivalent in terms of the total cumulative reward. Thus, for RL one policy is completely equivalent to its symmetric counterpart.

### 4.2 Heuristic analysis

We now discuss the role of the interval between decision times,  $\tau$ , by relying on the set of 81 heuristic (hard-wired) strategies obtained as a reduced policies space from the 4 longitudinal states and the first 3 actions in Fig. 1. Indeed, their analysis is enough to understand the qualitative effect of changing the decision time with no needed to perform any learning.

In Fig. 7, we show the same plot of Fig. 5 for different values of  $\tau$  and only considering the heuristic policies, taking the Pareto dominating strategies in this reduced policy space we obtain a lower bound to the true Pareto frontier, which is enough for the following analysis. Small decision values of  $\tau$  correspond to frequent measurements of the system and thus, as intuition would suggest, to major adjustments of the control variables that lead to high quality performances. In particular,  $\tau = 0.01 = dt$  (i.e., controlling at each time step,  $dt$ ) leads to a linear Pareto frontier,  $\langle R_\lambda \rangle \propto \langle R_A \rangle$ , where all policies are equivalent, meaning that they all live on the Pareto frontier: none (Pareto) dominates the others. For this specific value of  $\tau$ , we have also investigated what MORL can learn and we discovered that, on average, MORL solutions are indistinguishable from heuristics, since all of them fall on the linear frontier. It is reasonable to imagine that the linear frontier is optimal because whenever we allow the agent to update its direction continuously the optimal policies tend to be on the linear frontier. This is true either when  $\tau$  is 0, or when we have a finite interval between deci-

sion times but still a continuous update of the direction (not shown). On the other hand, all other best policies found for finite  $\tau$  and noncontinuous update of direction are sub-optimal with respect to the linear frontier. In other terms, if the Lagrangian pair can continuously sense its separation, it does not really need to search for optimal policies. Increasing the decision time values leads to concave frontiers where the strategies play different roles until  $\tau$  starts to be too large with respect to  $1/\lambda$  and swimming becomes ineffective in controlling the separation growth and it only represents an activation cost. For instance, for  $\tau = 1$  swimming does not help on minimizing the separation and thus swimming or being passive is almost equivalent.

To better understand the linear behavior at  $\tau \rightarrow 0$ , we can derive the following heuristic analysis. Since for the whole duration of an episode we are in the linear regime of separation (i.e., the agents see a differentiable velocity field), we know from (9) that  $-\langle R_\lambda \rangle$  is nothing but the Lyapunov exponent of the controlled system,  $\lambda_c$ . The actions of swimming along the joining direction introduce a clear contraction factor, so (if  $\tau$  is sufficiently small) we can estimate the controlled Lyapunov exponent for the heuristic policies as follows:

$$\lambda_c \simeq \frac{\lambda T_{\max} - (2f T_2 + f T_1)}{T_{\max}}, \tag{13}$$

where we have decomposed the total episode duration as  $T_{\max} = T_0 + T_1 + T_2$ , with  $T_1$  being the average time in which only one agent is swimming, while  $T_0$  and a  $T_2$  are the average times in which both agents are passive and swimming, respectively. For the *naïve* baseline  $T_2 = T_{\max}$ ,  $T_1 = T_0 = 0$  and we can estimate  $\lambda_{naïve} \simeq \lambda - 2f$  (if  $\tau \rightarrow 0$ ). This means that for  $\lambda \simeq 1.4$  and  $f = 0.7$  the *naïve* baseline should be very close to a *perfect control*, i.e., it can keep the distance constant. On the other hand, based on the same decomposition of the total time,  $\langle R_A \rangle$  can be approximated as

$$\langle R_A \rangle = -\frac{\lambda}{T_{\max}}(2T_2 + T_1), \tag{14}$$

which implies a linear dependence between  $\langle R_\lambda \rangle$  and  $\langle R_A \rangle$ :

$$\langle R_\lambda \rangle \simeq -\lambda - \frac{f}{\lambda} \langle R_A \rangle, \tag{15}$$

which explains the linearity of the Pareto frontier for  $\tau = dt$  in Fig. 7. When the above relation applies (i.e., for  $\tau \rightarrow 0$ ), we can write the total reward as

$$\langle R_{\text{tot}} \rangle \simeq -\lambda + \langle R_A \rangle \left( \beta - \frac{f}{\lambda} \right). \tag{16}$$

It is now clear why all the policies lie on the Pareto frontier, and thus are equivalent. For  $\beta < f/\lambda$ , the task is to minimize  $\langle R_A \rangle$  (remember that  $\langle R_A \rangle$  is negative

defined), that means controlling continuously the system applying the *naïve* policy. For  $\beta > f/\lambda$ , the goal is to maximize  $\langle R_A \rangle$ , which is maximal (i.e., equal to 0) when both agents are passive. For  $\beta = \beta_c = f/\lambda$  all policies perform the same,  $\langle R_{\text{tot}} \rangle \simeq -\lambda$ .

Clearly, the linearity of the frontier is due to the choice of the swimming penalization we adopted (Cfr. Eq. (10)), which is linear in the number of swimming agents. Different (nonlinear) choices would break the linearity but will not invalidate the decomposition we used above. In this paper, we are not interested in exploring other definition of rewards and we have chosen the simplest definition, which is enough to highlight the nontrivial role played by the discrete decision time. Indeed it is due to such discreteness that the agents need to learn how to exploit the flow in an intelligent way and where different policies are not equivalent anymore in terms of performances.

## 5 Discussions and conclusions

We have presented a multi-agent and multi-task problem set to minimize, at the same time, the dispersion rate of a Lagrangian pair dominated by Lagrangian Chaos, in a stochastic flow, and the activation cost due to the active control on the system. We modeled the agents with limited observation capabilities, 16 states inform them on the longitudinal and transversal velocity gradients in a discretized form, and with a set of 15 possible choices of action for the agent pair. Thus, the space of deterministic policies is very large and counts  $15^{16}$  navigation strategies. Furthermore, the agents could swim with a variable but limited velocity intensity, namely they were not able to overcome the chaoticity properties of the system. To solve this problem, we have developed a MORL approach based on the combination of the simple Q-learning algorithm and the scalarization technique; this enabled us to show a systematic investigation of the problem studying the Pareto frontier. In this direction, we have shown how controlling only at discrete decision times makes the problem nontrivial. Indeed, the larger the interval between decision times is the more control variables performances become unpredictable or, at least, not easy to guess a priori. In the limit of continuous control,  $\tau \rightarrow 0$ , the problem reduces to a linear Pareto frontier, where all policies are equivalent (i.e., they all live on the frontier), while increasing  $\tau$  the frontier becomes concave and the strategies play different roles in minimizing the separation. Instead, for high decision time,  $\tau \gg 1/\lambda$ , with  $\lambda$  the Lagrangian Lyapunov exponent of the system, swimming becomes ineffective to control the pair separation. We stress that the MORL technique here implemented is model-free, as it requires only a few local and instantaneous information about the underlying flow to define the set of states and actions, while from the other requires nonlocal information to define the agents dynamics. In fact, the particles swim by continuously resetting their con-

trol variables equal to the ones chosen at the last decision time, reacting instantaneously to the underlying flow. Remarkably, we showed that, within our setup, RL is able to reach solutions that are strongly different from a *naïve* baseline and, in general, they are different from heuristic references based on “longitudinal” actions only. It would be important to extend the present approach to the case of smart tracers able to control their separation within scales where velocity field is no more differentiable, i.e., in the inertial range of turbulent flows.

**Acknowledgements** This work was supported by the European Research Council (ERC) under the European Union’s Horizon 2020 research and innovation programme (Grant Agreement No. 882340).

## Author contribution statement

All authors conceived the research. CC performed all the numerical simulations and data analysis. All authors discussed the results. CC wrote the paper with revision and input from all the authors.

**Data availability statement** Data sharing not applicable to this article as no datasets were generated or analysed during the current study.

## Appendix A: Q-learning implementation

To solve the optimization problem, we used the Q-learning algorithm [35] which is based on evaluating the action-value function,  $Q(s, a)$ , that is the expected future cumulative reward given that the agents are in state  $s$  and take action  $a$ . The algorithm is expected to converge to the optimal policy by the following iterative trial-and-error protocol. At each decision time  $t_j$ , the agents pair measures its state  $s_{t_j}$  and selects an action  $a_{t_j}$  using an  $\epsilon$ -greedy strategy, where  $a_{t_j}(s_{t_j}) = \arg \max_a \{Q(s_{t_j}, a)\}$  with probability  $1 - \epsilon$  or  $a_{t_j}$  is chosen randomly with probability  $\epsilon$ . Then, we let the dynamical system evolve for a time  $\tau$ , according to (1), keeping both control directions and velocity intensity fixed. Afterward, the agents receive a reward  $r_{\text{tot}}(t_{j+1})$  (11) and the Q-matrix is updated as

$$Q(s_{t_j}, a_{t_j}) \leftarrow Q(s_{t_j}, a_{t_j}) + \alpha [r_{\text{tot}}(t_{j+1}) + \max_a Q(s_{t_{j+1}}, a) - Q(s_{t_j}, a_{t_j})], \quad (17)$$

where  $\alpha$  is the learning rate. Updates are repeated up to the end of the episode  $t = T_{\text{max}}$ , when no reward is assigned. The learning protocol is repeated restarting with another pair with the same initial distance in another flow position until we reach a “local” optimum given by the equation  $Q^*(s_{t_j}, a) = r_{\text{tot}}(t_{j+1}) + \max_a Q^*(s_{t_{j+1}}, a)$  and defined by the policy

$$a(s) = \arg \max_a \{Q^*(s, a)\}.$$

In order to ease the convergence of the algorithm, the learning rate  $\alpha$  is taken as a decreasing functions of the time spent in the state-action pair, while the exploration parameters decrease with the time spent in the visited state. Thus if  $n(s, a)$  is the number of decision times in which the couple  $(s, a)$  has been visited, and

$$n(s) = \sum_a n(s, a)/|\mathcal{A}|, \quad (18)$$

$\epsilon$  and  $\alpha$  are taken as:

$$\alpha = 5/[200^{1/\gamma} + \tau n(s, a)]^\gamma \quad (19)$$

$$\epsilon = 5/[200^{1/\gamma} + \tau n(s)]^\gamma \quad (20)$$

with  $\gamma = 4/5$ , the numerical values of the constants have been determined after some preliminary tests. As for the initialization of the matrix  $Q$ , we have taken the same large (optimistic) value for all the state-action pairs.

## References

- P. Lermusiaux, D. Subramani, J. Lin, C.S. Kulkarni, A. Gupta, A. Dutt, T. Lolla, P.J. Haley Jr., W. Hajj Ali, C. Mirabito, S. Jana, A future for intelligent autonomous ocean observing systems. *J. Mar. Res.* **75**, 765–813 (2017)
- Y. Elor, A.M. Bruckstein, Two-robot source seeking with point measurements. *Theor. Comput. Sci.* **457**, 76–85 (2012)
- W. Wu, I.D. Couzin, F. Zhang, Bio-inspired source seeking with no explicit gradient estimation. *IFAC Proceedings Volumes* **45**(26), 240–245 (2012). (**3rd IFAC Workshop on Distributed Estimation and Control in Networked Systems**)
- FSTaxis Algorithm: Bio-Inspired Emergent Gradient Taxis, volume ALIFE 2016, the Fifteenth International Conference on the Synthesis and Simulation of Living Systems of ALIFE 2022: The 2022 Conference on Artificial Life, 07 (2016)
- C. Bechinger, R. Di Leonardo, H. Löwen, C. Reichhardt, G. Volpe, G. Volpe, Active particles in complex and crowded environments. *Rev. Mod. Phys.* **88**(4), 045006 (2016)
- A. Crisanti, M. Falcioni, A. Vulpiani, G. Paladin, Lagrangian chaos: transport, mixing and diffusion in fluids. *Riv. Nuovo Cim.* **14**(12), 1–80 (1991)
- M. Cencini, F. Cecconi, A. Vulpiani, *Chaos: From Simple Models to Complex Systems. Series on Advances in Statistical Mechanics* (World Scientific, Singapore, 2010)
- F. Ginelli, The physics of the vicsek model. *Eur. Phys. J. Spec. Top.* **225**(11), 2099–2117 (2016)
- M.C. Marchetti, J.F. Joanny, S. Ramaswamy, T.B. Liverpool, J. Prost, M. Rao, R. Aditi Simha, Hydrodynamics of soft active matter. *Rev. Mod. Phys.* **85**, 1143–1189 (2013)
- M. Ballerini, N. Cabibbo, R. Candelier, A. Cavagna, E. Cisbani, I. Giardina, V. Lecomte, A. Orlandi, G. Parisi, A. Procaccini, M. Viale, V. Zdravkovic, Interaction ruling animal collective behavior depends on topological rather than metric distance: Evidence from a field study. *Proc. Natl. Acad. Sci.* **105**(4), 1232–1237 (2008)
- N. Khurana, N.T. Ouellette, Stability of model flocks in turbulent-like flow. *New J. Phys.* **15**(9), 095015 (2013)
- L. Biferale, F. Bonaccorso, M. Buzicotti, P. Clark Di Leoni, K. Gustavsson, Zermelo’s problem: Optimal point-to-point navigation in 2d turbulent flows using reinforcement learning. *Chaos* **29**(10), 103138 (2019)
- M. Buzicotti, L. Biferale, F. Bonaccorso, P. Clark di Leoni, K. Gustavsson. Optimal control of point-to-point navigation in turbulent time dependent flows using reinforcement learning, in *AIxIA 2020—Advances in Artificial Intelligence*, 223–234. (Springer, Cham, 2021)
- J.K. Alageshan, A.K. Verma, J. Bec, R. Pandit, Machine learning strategies for path-planning microswimmers in turbulent flows. *Phys. Rev. E* **101**, 043110 (2020)
- G. Reddy, A. Celani, T.J. Sejnowski, M. Vergassola, Learning to soar in turbulent environments. *Proc. Natl. Acad. Sci.* **113**(33), E4877–E4884 (2016)
- G. Reddy, J. Wong-Ng, A. Celani, T.J. Sejnowski, M. Vergassola, Glider soaring via reinforcement learning in the field. *Nature* **562**(7726), 236–239 (2018)
- N. Orzan, C. Leone, A. Mazzolini, J. Oyero, A. Celani. Optimizing airborne wind energy with reinforcement learning. *Europ. Phys. J. E* **46**, 2 (2023)
- S. Verma, G. Novati, P. Koumoutsakos, Efficient collective swimming by harnessing vortices through deep reinforcement learning, in *Proceedings of the National Academy of Sciences of the United States of America* **115**(23), 5849–5854 (2018)
- Z. Zou, Y. Liu, Y.N. Young, O.S. Pak, A.C.H. Tsang, Gait switching and target navigation of microswimmers via deep reinforcement learning. *Commun. Phys.* **5**(1), 158 (2022)
- J. Qiu, N. Mousavi, L. Zhao, K. Gustavsson, Active gyrotactic stability of microswimmers using hydromechanical signals. *Phys. Rev. Fluids* **7**(1), 014311 (2022)
- A. Daddi-Moussa-Ider, H. Löwen, B. Liebchen, Hydrodynamics can determine the optimal route for microswimmer navigation. *Commun. Phys.* **4**, 15 (2021)
- F. Borra, L. Biferale, M. Cencini, A. Celani, Reinforcement learning for pursuit and evasion of microswimmers at low Reynolds number. *Phys. Rev. Fluids* **7**(2), 023103 (2022)
- G. Zhu, W. Fang, L. Zhu, Optimizing low-Reynolds-number predation via optimal control and reinforcement learning. *J. Fluid Mech.* **944**, A3 (2022)
- S. Goh, R. Winkler, G. Gompper, Noisy pursuit and pattern formation of self-steering active particles. *New J. Phys.* **24**, 093039 (2022)
- C.A.C. Coello. Handling preferences in evolutionary multiobjective optimization: a survey, in *Proceedings of the 2000 Congress on Evolutionary Computation. CEC00 (Cat. No.00TH8512)*, vol. 1 (2000), pp. 30–37
- C. Coello, D. Veldhuizen, G. Lamont. *Evolutionary Algorithms for Solving Multi-Objective Problems Second Edition* (Springer US, 2007)
- C. Liu, X. Xu, D. Hu, Multiobjective reinforcement learning: a comprehensive overview. *IEEE Trans. Syst. Man Cybern. Syst.* **45**(3), 385–398 (2015)
- P. Vamplew, R. Dazeley, A. Berry, R. Issabekov, E. Dekker, Empirical evaluation methods for multiobjective reinforcement learning algorithms. *Mach. Learn.* **84**(1–2), 51–80 (2011)
- S. Natarajan P. Tadepalli. Dynamic preferences in multi-criteria reinforcement learning, in *Proceedings of the*

- 22nd International Conference on Machine Learning, ICML'05* (Association for Computing Machinery, New York, NY, USA, 2005), pp. 601–608
30. A. Castelletti, G. Corani, A.E. Rizzoli, R. SonciniSessa, E. Weber, *Reinforcement Learning in the Operational Management of a Water System* (Pergamon Press, Oxford, 2002), p.325
  31. P. Vamplew, J. Yearwood, R. Dazeley, A. Berry. On the limitations of scalarisation for multi-objective reinforcement learning of pareto fronts, in *AI 2008: Advances in Artificial Intelligence* (Springer Berlin Heidelberg, 2008), pp. 372–378
  32. E. Zitzler, L. Thiele, M. Laumanns, C.M. Fonseca, V.G. da Fonseca, Performance assessment of multiobjective optimizers: an analysis and review. *IEEE Trans. Evol. Comput.* **7**(2), 117–132 (2003)
  33. J. Bec, Multifractal concentrations of inertial particles in smooth random flows. *J. Fluid Mech.* **528**, 255–277 (2005)
  34. C.W. Gardiner, *Handbook of Stochastic Methods for Physics, Chemistry, and the Natural Sciences. Springer complexity* (Springer, Berlin, 2004)
  35. R.S. Sutton, A.G. Barto, *Reinforcement Learning: An Introduction* (MIT Press, Cambridge, 2018)

Springer Nature or its licensor (e.g. a society or other partner) holds exclusive rights to this article under a publishing agreement with the author(s) or other rightsholder(s); author self-archiving of the accepted manuscript version of this article is solely governed by the terms of such publishing agreement and applicable law.